Gravity wave spectra in the lower stratosphere diagnosed from project loon balloon trajectories

M. R. Schoeberl, E. Jensen, A. Podglajen, L. Coy, C. Lodha, S. Candido, R. Carver

AGU PUBLICATIONS

JGR

Journal of Geophysical Research: Atmospheres

RESEARCH ARTICLE
10.1002/2017JD026471

Key Points:
- Project Loon superpressure balloons provide unique information about lower stratospheric gravity waves
- The wave energy spectrum roughly follows a −2 power law nearly everywhere
- The amplitude of the temperature fluctuations with periods shorter than a day is higher than some previous estimates

Correspondence to:
M. R. Schoeberl,
mark.schoeberl@mac.com

Citation:
Schoeberl, M. R., E. Jensen, A. Podglajen, L. Coy, C. Lodha, S. Candido, and R. Carver (2017), Gravity wave spectra in the lower stratosphere diagnosed from project loon balloon trajectories, *J. Geophys. Res. Atmos.*, *122*, 8517–8524, doi:10.1002/2017JD026471.

Received 9 JAN 2017
Accepted 7 AUG 2017
Accepted article online 14 AUG 2017
Published online 23 AUG 2017

Gravity wave spectra in the lower stratosphere diagnosed from project loon balloon trajectories

M. R. Schoeberl[1], E. Jensen[2], A. Podglajen[3,4], L. Coy[5,6], C. Lodha[7], S. Candido[7], and R. Carver[7]

[1]Science and Technology Corporation, Columbia, Maryland, USA, [2]NASA Ames Research Center, Moffett Field, California, USA, [3]Laboratoire de Météorologie Dynamique, CNRS-UMR8539, Institut Pierre Simon Laplace, École Normale Supérieure, École Polytechnique, Université Pierre et Marie Curie, Paris, France, [4]Laboratoire de Météorologie Dynamique/IPSL, UPMC Univ Paris 06, CNRS, Palaiseau, France, [5]NASA Goddard Space Flight Center, Greenbelt, Maryland, USA, [6]SSAI, Lanham, Maryland, USA, [7]Project Loon, X, Mountain View, California, USA

Abstract Project Loon has been launching superpressure balloons since January 2013 to provide worldwide Internet coverage. These balloons typically fly between 18 and 21 km and provide measurements of winds and pressure fluctuations in the lower stratosphere. We divide 1560 Loon flights into 3405 two-day segments for gravity wave analysis. We derive the kinetic energy spectrum from the horizontal balloon motion and estimate the temperature perturbation spectrum (proportional to the potential energy spectrum) from the pressure variations. We fit the temperature (and kinetic energy) data to the functional form $T'^2 = T'_o{}^2[\omega/\omega_o)^\alpha$, where ω is the wave frequency, ω_o is daily frequency, T'_o is the base temperature amplitude, and α is the spectral slope. Both the kinetic energy and temperature spectra show -1.9 ± 0.2 power-law dependence in the intrinsic frequency window 3–50 cycles/day. The temperature spectrum slope is weakly anticorrelated with the base temperature amplitude. We also find that the wave base temperature distribution is highly skewed. The tropical modal temperature is 0.77 K. The highest amplitude waves occur over the mountainous regions, the tropics, and the high southern latitudes. Temperature amplitudes show little height variation over our 18–21 km domain. Our results are consistent with other limited superpressure balloon analyses. The modal temperature is higher than the temperature currently used in high-frequency gravity wave parameterizations.

Plain Language Summary Using Project Loon balloon trajectories, we present new observations of the lower stratospheric gravity wave spectra.

1. Introduction

Gravity waves play and important role in upper atmosphere dynamics as a driver of the upper stratospheric and mesospheric circulation [*Fritts and Alexander*, 2003, and references therein]. More recently, gravity waves have been recognized as a key component in cloud formation in the upper troposphere [*Jensen and Pfister*, 2004; *Schoeberl et al*., 2014] and the polar stratosphere [*Alexander et al*., 2013; *Orr et al*., 2015]. Our knowledge of these gravity wave fluctuations is limited, especially in the lower stratosphere and upper troposphere; thus, any new information on the distribution and intensity of these waves is useful. In this paper we report on the analysis of Loon superpressure balloon data. The Loon data provide a new and extensive source of information on gravity waves in the lower stratosphere.

Analysis of gravity waves observed by aircraft and superpressure balloons is described in a number of papers [e.g., *Bacmeister et al*., 1996, *Hertzog and Vial*, 2001; *Vincent et al*., 2007]. *Boccara et al*. [2008] and *Podglajen et al*. [2016] detail the current approach to Lagrangian analysis of superpressure balloon data. The Boccarra et al. approach has been applied to Strateole/Vorcore and Concordiasi balloon campaigns with the goal of assessing the upward momentum flux of gravity waves in the South Polar regions [*Hertzog et al*., 2008]. These superpressure balloon data have also been used to evaluate reanalysis fields [*Podglajen et al*., 2014; *Friedrich et al*., 2017].

The particular focus of this work is not the momentum fluxes but the pressure (temperature) fluctuations produced by gravity waves in the lower stratosphere and their potential impact on cloud formation and stratospheric dehydration. Stratospheric dehydration occurs as air rising from the tropical upper troposphere into the stratosphere passes through the cold tropical tropopause layer [*Fueglistaler et al*., 2009]. Water vapor is removed through cloud formation and the sedimentation of ice crystals. Gravity wave temperature

fluctuations fine-tune this process by further suppressing the minimum temperature [*Kim and Alexander*, 2015] and affecting the ice crystal number and particle size distribution [*Jensen et al*., 2012; *Spichtinger and Krämer*, 2013; *Kärcher et al*., 2014; *Dinh et al*., 2016; *Jensen et al*., 2016; *Schoeberl et al*., 2016].

In Lagrangian models of stratospheric dehydration, the high-frequency gravity wave temperature fluctuations are added to the reanalysis temperature field [*Jensen and Pfister*, 2004; *Schoeberl et al*., 2016] because these fluctuations are muted in the reanalysis fields. Thus, Loon data will help us better determine how to parameterize high-frequency gravity waves in the Lagrangian models. Although our primary interest is in tropical gravity measurements, most of the Loon data are extratropical, so we extend our data analysis to the extratropical regions.

2. Description of the Project Loon Data

Project Loon, hereafter referred to as Loon, has an overall goal of providing worldwide Internet coverage using a network of long-duration superpressure balloons. These balloons, floating between 17 and 21 km, can form a network linked to a ground-based telecom provider. Increasing or decreasing the pressure inside the balloon can adjust the float altitude. Thus, the Loon balloons can navigate by changing altitude into different wind regimes. Loon launches began in 2013 and continue to the present. Our database consists of 1664 flights, of which 1560 are long enough for analysis. These flights occurred from January 1, 2013 through December 31, 2016. Loon balloons do not have permission to fly everywhere, and they are cut when they cannot avoid restricted regions. Nonetheless, there is good coverage in the Southern Hemisphere midlatitudes and partial coverage of the Northern Hemisphere midlatitudes and the tropics. Loon measurements add significantly to the data provided by previous superpressure balloon experiments such as Concordiasi [*Rabier et al*., 2010].

Each Loon balloon has a solar powered payload that includes a GPS position sensor, a pressure sensor, a surface pointing radiometer, and balloon gas temperature sensor [*Friedrich et al*., 2017]. Data from these sensors are recorded at 1–2 minute intervals with occasional gaps due to telemetry dropouts. We restrict ourselves to the GPS position and pressure sensor data since the balloon gas temperature is a poor indicator of the atmospheric temperature. Loon has provided an upper bound on the uncertainties of the sensors: 1.5 hPa for pressure and 10 m for GPS location. Loon winds are derived from the changes in position. The GPS uncertainty suggests an accuracy upper bound of 0.33 m/s on the derived wind speed.

3. Analysis of the Loon Data

We restrict our analysis to the 18–21 km region that has the highest density of balloon data. We examine each balloon flight and discard very short flights or obviously bad data sets. We remove time gaps in the data, abutting data sets if possible. We next remove the pressure jumps associated with navigation, or our data abutments. To remove the jumps, we take the time derivative of the balloon pressure altitude and screen for anomalously high derivatives. We then set the anomalous derivatives to zero and reconstruct the balloon pressure integrating the derivative forward in time. This approach effectively knits together the data stream, removing the jumps; however, it can create altitude biases in the data—that is, the data will be reported at only one altitude. This bias could be important if we believe that the gravity wave amplitudes vary significantly within our altitude domain. To test for this possibility, we have narrowed our vertical domain and repeated our analyses. We found that our results show little variation in wave amplitude with altitude within the narrowed vertical domains, consistent with other studies [e.g., *Kim and Alexander*, 2013]. This result suggests that the introduced altitude bias is unimportant.

Each balloon flight is subdivided into 2 day intervals—long enough to resolve the pressure fluctuation frequency at 1 cycle/day and higher. Any linear wind trend over the segment is removed, and the data are interpolated onto a regular time grid. We use each segment's average position to tag longitude, latitude, and height of the segment as shown in figures below. From 1560 usable balloon flights, we have extracted 3405 two-day segments that fit within the altitude domain 18–21 km. Figure 1 shows a sample of Loon data from a single segment. The figure shows the location of the balloon segment and the wind and log-pressure altitude z ($H \log_e(p_s/p)$, where H is the scale height, ~7 km; p is pressure; and p_s is a reference pressure, 1000 hPa). From these data, we compute the Lagrangian kinetic energy and temperature power spectrum as shown in Figure 1. Our approach is identical to that used by *Podglajen et al*. [2016]. We assume that the

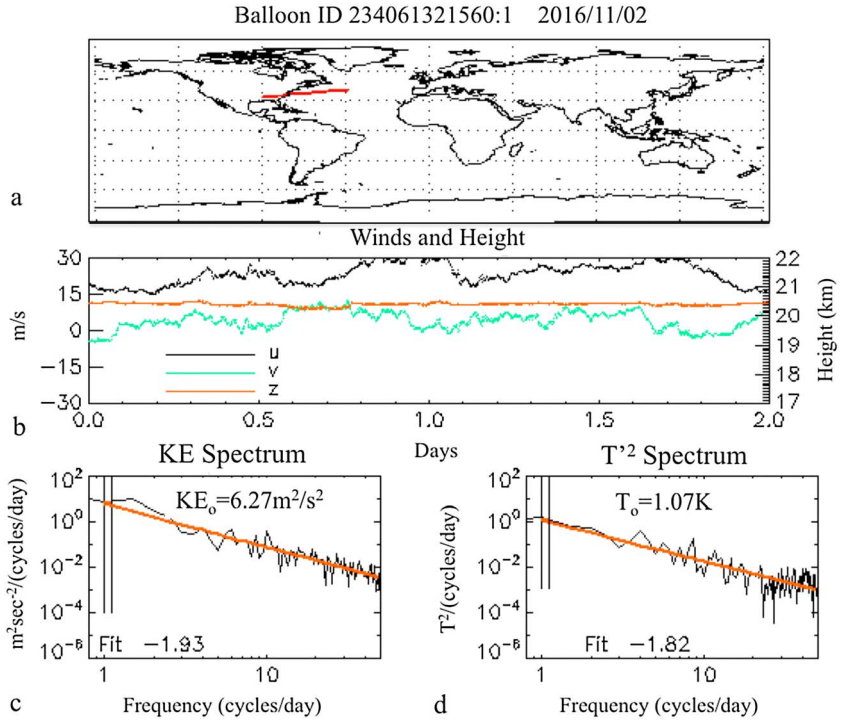

Figure 1. Sample analysis of a single balloon segment with the indicated flight date and ID. (a) Balloon flight path for this 2 day flight segment. (b) Wind speed and log-pressure altitude of the balloon. (c) *KE* and (d) T'^2 spectrum, the 1 cycle/day value, and the fit derived from data between 3 and 50 cycles/day. The vertical lines in Figures 1c and 1d show the averaging region used to generate KE_o and T'_o.

balloon isopycnic perturbation vertical displacement, ζ'_B, is related to the isentropic vertical displacement, $\zeta_B = \sigma\zeta'$, where σ is ~0.3 [*Vincent and Hertzog*, 2014; *Podglajen et al.*, 2014]. Primes indicate perturbations from the mean. Next, we relate the isentropic vertical displacement to the Lagrangian temperature fluctuations assuming (dry) adiabatic expansion, $T' = -\zeta' g/C_p$, where C_p is the specific heat of dry air at constant pressure and g is the acceleration due to gravity.

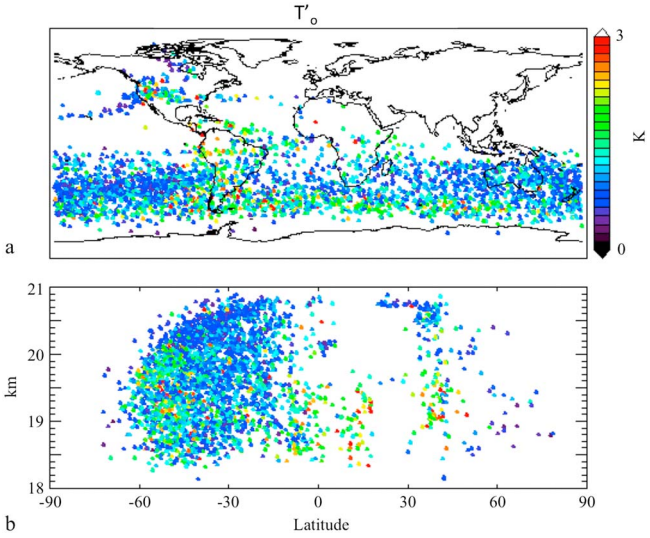

Figure 2. Distribution of T'_o values from individual 2 day balloon segments. (a) Spatial distribution; (b) distribution with altitude. For each segment the spatial position shown as a colored dot is the average latitude, longitude, and height of the balloon track.

The kinetic energy (*KE*) can be obtained from the horizontal velocities; the kinetic energy contribution by with vertical wind is much smaller and can be neglected. The potential energy E_p is related to the vertical displacement and hence the temperature perturbation, $E_P = {}^1/_2(C_P N/g)^2 T'^2$, where N is the buoyancy frequency. Instead of computing the potential energy, we focus on T'^2 since that is the relevant quantity for cloud dehydration. After computing the power spectrum as a function of frequency for *KE* and T'^2, we model the temperature and *KE* spectrum as $T'^2 = T'_o{}^2(\omega/\omega_o)^\alpha$ and $KE = KE_o(\omega/\omega_o)^\alpha$, where α is the fit for

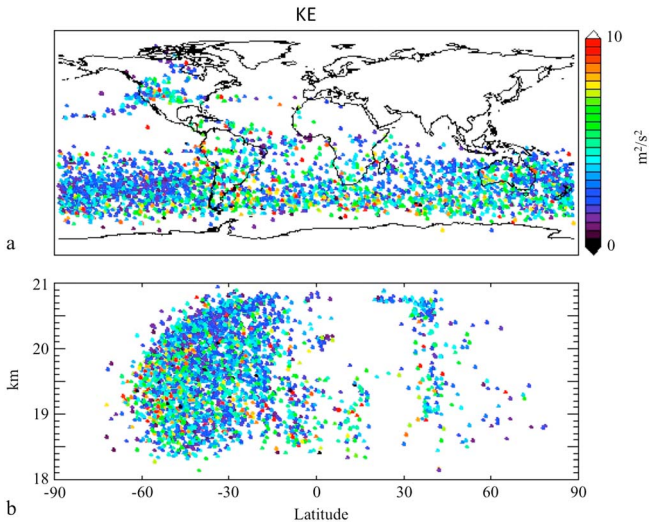

Figure 3. As in Figure 2, but the distribution of KE_o values from individual 2 day balloon segments. (a) Spatial distribution; (b) distribution with altitude.

frequencies between 3 and 50 cycle/day and T'_o and KE_o are the value at frequency ω_o, 1 cycle/day. Figure 1 shows an example of such a fit extended to 1 cycle/day from the 3–50 cycles/day data. As shown by *Massman* [1978], *Dinh et al*. [2016], and *Podglajen et al*. [2016], inertial superpressure balloon motions occur at a much higher frequency than our fit region and therefore do not contaminate our results. The value of T'_o is determined by averaging the data between 1 and 1.1 cycles/day, shown as vertical bars in the figure, or T'_o can be determined from the 3–50 cycles/day fit by extrapolating the fit to 1 cycle/day. Both methods give nearly the same value. α values (labeled fit in the figure) are also shown.

4. Results

4.1. Spectrum Slope and T'_o Distributions

To get a good idea of the distribution of high-frequency waves in the upper troposphere-lower troposphere region, we plot T'_o as a function of latitude-longitude (Figure 2a) and latitude-height (Figure 2b). The average position of each balloon over the 2 day segment is shown as a colored dot. Figures 3a and 3b show the KE_o distribution. The highest concentration of Loon segments is in the Southern Hemisphere, where the balloons were quite long lived. The largest values for T'_o and KE_o values appear to be located over topography in both hemispheres (the Rockies and South America) and near the high southern latitudes near the roaring 40s. This result is consistent with other gravity wave measurements over steep topography by balloons, rockets, and satellites [e.g., *Alexander*, 1998; *Eckermann et al*., 1999; *Hertzog et al*., 2008; *Alexander et al*., 2013, *Orr et al*., 2015], and we might expect enhanced gravity wave generation over the strong southern hemisphere jet [*Fritts and Nastrom*, 1992]. The height distribution of T'_o and KE_o (Figures 2b and 3b) shows highest values in the Southern Hemisphere with scattered large values in the north and a few large anomalies in the tropics. In general, the T'_o appears to be less noisy than the kinetic energy spectrum.

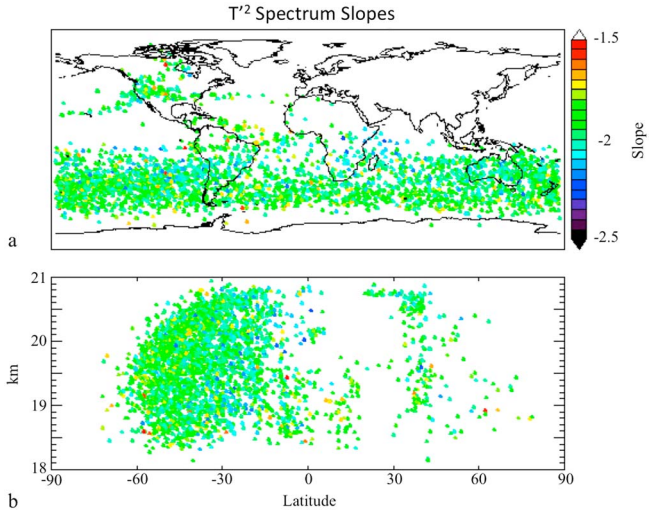

Figure 4. As in Figure 2, but the distribution of T'^2 spectrum slopes from individual 2 day balloon segments. (a) Spatial distribution; (b) distribution with altitude.

Analysis of the wave amplitudes with height (not shown) shows that the magnitude of the waves is roughly constant between 18.6 and 21 km. *Kim and Alexander* [2013] analyzed high-frequency tropical radiosonde temperature variations due to atmospheric waves. They showed that the temperature variance decreased by only by 16% from 18 to 21 km. Their results are consistent with our assessment that the gravity wave amplitudes do not show much change with altitude in the lower stratosphere.

Figure 4 shows the distribution of spectral slopes for T'^2. Most of the spectrum follows the -2 or slightly shallower

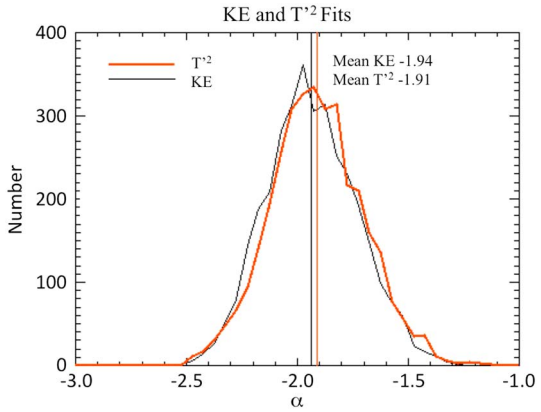

Figure 5. PDF of α values (slopes) for *KE* and T'^2 fits from all Loon 2 day segments. Mean values are the vertical lines.

slope even in high amplitude wave regions as seen in Figures 2 and 3. The correlation between T'_o and the spectrum slope is −0.38; in other words, weaker anomalies tend to have shallower slopes, and the spectrum tends to be redder with stronger anomalies. Figure 5 shows the distribution of all spectrum fits. The T'^2 and *KE* fits are computed independently in our analysis; however, they have very similar distributions. This gives us confidence in our analysis since the kinetic and potential energy are related through the gravity wave polarization relations and should have similar slopes except where the frequency approaches either the buoyancy frequency (which is outside of our fit range) or the Coriolis frequency [*Fritts and Alexander*, 2003; *Podglajen et al*., 2016]. We note that the T'^2 mean slope is about −1.91 ± 0.2 (half-max) with a slope range between −1.3 and −2.5; the *KE* distribution shows similar behavior. The spread in slopes in Figure 3 is likely due to uncertainties in the power spectrum fit. *Hertzog and Vial*'s [2001] analysis of the Ecuador balloon campaign data also noted the ubiquitous −2 power law in the *KE* spectrum as did *Bacmeister et al*. [1996] in their analysis of aircraft data. In fact, the −2 high-frequency gravity wave spectral slope power law behavior appears to be fairly universal [*Fritts and VanZandt*, 1993, and references therein]. Most authors agree that the *KE* and E_p −2 power law behavior is likely the result of the energy cascade between scales associated with 2-D turbulence [*Dewan*, 1994; *Dewan et al*., 1992; *Smith et al*., 1987; *Gage*, 1979] (also see discussion in *Bacmeister et al*. [1996]).

Figure 6 shows T'_o distribution as a function of segment length. The distribution is quite skewed as previously observed for waves at very high southern latitudes [*Baumgaertner and McDonald*, 2007; *Alexander et al*., 2013]. In other words, the mean is strongly weighted by the anomalous high amplitude events. The KE_o distribution (not shown) has a similar behavior. The mean and mode T'_o values are shown in the figure. The mode (0.77 to 0.45 K) is ~0.3 K smaller than the mean; both the mean and the mode vary with segment length—increasing for shorter segments. The reason for the variation in mean and mode with segment length is that longer segments are composites of data from shorter segments and the compositing tends reduce the influence of the high amplitude events. Because the mode is the most frequent observed value, it makes sense to use the mode to characterize the high-frequency wave amplitudes in model parameterizations rather than the mean. Seasonal variations in T'_o mean, mode, and standard deviation values are shown in Figure 7. The usual seasonal divisions are used, DJF, MAM, JJA, and SON. The data are grouped into 10° latitude zones, and we use 0.1 K temperature bins to determine the mode. Means are shown as black dots, and the mode is shown in red. Consistent with Figure 6, the modal values are almost always below the mean value T'_o values. Gravity wave amplitudes are systematically higher over the southern hemisphere midlatitudes with the exception of northern hemisphere winter. (We are probably

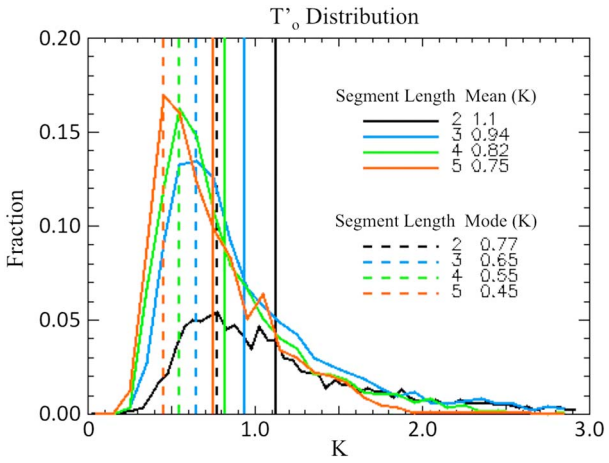

Figure 6. Normalized PDF of T'_o for all the Loon data using different segment lengths. The mean is shown as solid vertical lines and the mode as dashed lines. The caption shows the mean and mode values for different segment lengths: 2, 3, 4, and 5 days.

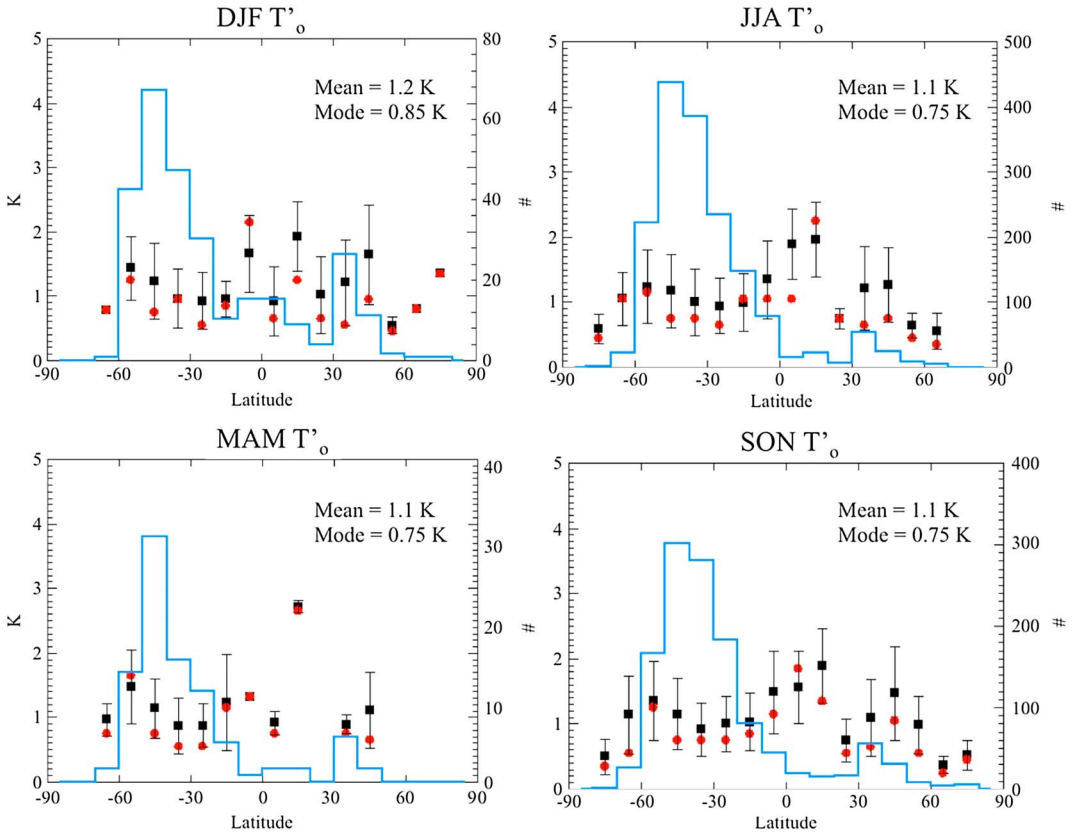

Figure 7. T'_o distribution as a function of latitude for the four seasons, DJF, MAM, JJA, and SON as indicated in the titles. The points show the mean value with the vertical bars marking ±1 standard deviation. The red dots show the modal values for each latitude bin. The blue lines indicate the number of measurements in each bin; the number scale is shown on the right-hand axis. The seasonal average mean and mode is shown in the upper right for each subfigure.

underestimating the winter wave amplitudes at high northern latitudes because few Loon balloons flew over the North Atlantic where Greenland's topography is expected to generate large amplitude mountain waves.) In JJA and SON tropical gravity wave values are high, suggesting the influence of convection, but there is too little data to draw a definite conclusion. Overall, our seasonal variation is broadly consistent with the gravity wave climatology of *Alexander* [1998].

4.2. Comparison with Other Estimates

Table 1 compares various estimates of the gravity wave temperature amplitudes in the lower stratosphere. As noted above, recent Lagrangian models of stratospheric dehydration [*Jensen and Pfister*, 2004; *Ueyama et al.*, 2015; *Schoeberl et al.*, 2014, 2016] add high-frequency gravity waves to the reanalysis fields (e.g., MERRA-2) [*Bosilovich et al.*, 2015; *Molod et al.*, 2015]. The reanalysis fields are available at 6 hour intervals; therefore, the reanalysis cannot realistically represent high-frequency waves. Computing the power spectrum of the wind and pressure fluctuations along a Lagrangian isentropic trajectory using MERRA and MERRA-2 data, we find lower T'_o values and a much steeper spectrum slope than indicated by our analysis of Loon data

Table 1. Comparison of Base T'_o Values at 1 Cycle/Day and the Spectrum Slope, α

Source	T'_o(K)	
MERRA Tropics (NH winter)	0.174	−3.61
MERRA-2 Tropics (NH winter)	0.17	−3.59
Jensen and Pfister [2004]	~0.4	−1.85
Schoeberl et al. [2016]	0.1	−2
Podglajen et al. [2016]		
S. Pole	0.90	−1.78
Tropics	1.07	−1.96
Loon	Mean, mode	
NH midlatitudes	1.22, 0.775	−1.89
SH midlatitudes	1.13, 0.625	−1.91
Tropics	1.23, 0.775	−1.88

(Table 1), which demonstrates the need to add the high-frequency gravity waves to the reanalysis fields.

Kim and Alexander [2013, 2015] argued that gravity waves effectively suppress the temperature below the time-averaged cold point. If the water vapor in the stratosphere is fixed at the coldest temperature an air parcel experiences when crossing the tropopause, then 0.7 K reduction in temperature—about the size of the waves observed—would lower stratospheric water by ~0.5 ppmv, about 12% of the stratospheric average value; gravity waves are clearly important. *Schoeberl et al*. [2015], among others, argued that the cloud nucleation process complicates the gravity wave dehydration for high-frequency waves so simply using the temperature suppression probably overestimates the effect of high-frequency waves on water vapor. In fact, as *Schoeberl et al*. [2016] show, these waves play a more significant role in controlling tropical cirrus cloud fraction than in dehydration. *Jensen et al*. [2016] came to the same conclusion. Table 1 compares model gravity wave amplitudes used by *Jensen and Pfister* [2004] (also used by *Ueyama et al*. [2015] and *Schoeberl et al*. [2016]). The T'_o values shown in Table 1 are much smaller than observations reported in this paper. Table 1 also shows that our assessment of the gravity wave amplitudes is in agreement with the analysis of the PreConcordiasi data by *Podglajen et al*. [2016].

5. Summary and Discussion

Project Loon has launched more than 1560 superpressure balloons more or less continuously since 2013. These balloons float in the lower stratosphere between 18 and 21 km. We have analyzed the wind and pressure fluctuations that are part of the Project Loon tracking data. Each Loon flight is divided into 2 day segments yielding 3259 data sets. We have analyzed the *KE* and T'^2 spectrum for frequencies greater than 3 cycles/day and less 50 cycles/day following the approach of *Podglajen et al*. [2016]. We fit the data to the functional form $T'^2 = T'^2_o(\omega/\omega_0)^\alpha$ for both *KE* and T'^2. We find that α is -1.92 ± 0.2 for T'^2 and -1.94 ± 0.2 for *KE*; the spectrum slope is roughly independent of latitude and altitude (Figure 4), although there is a weak anticorrelation between the slope and the base amplitudes (T'_o and KE_o). Steeper slopes are associated with stronger anomalies. The T'_o and KE_o distributions are highly skewed, and it is probably best to use the modal amplitudes rather than the mean amplitude to represent high-frequency waves in models. Table 1 shows the modal and mean T'_o and α values for different regions.

The Loon data show higher wave amplitudes over topography, the Austral subpolar regions, and in the tropics (Figures 2 and 3), which is consistent with many previous studies. Even though our analysis focuses on the lower stratosphere—just above the tropical tropopause, below the tropical tropopause, the gravity wave amplitudes are expected to decrease at lower altitudes [*Kim and Alexander*, 2013].

Our results (Table 1) agree with the PreConcordiasi superpressure balloon assessment of gravity wave amplitudes reported by *Podglajen et al*. [2016]. From our observations, Lagrangian models of stratospheric dehydration [*Schoeberl et al*., 2016; *Ueyama et al*., 2015] are adding too little high-frequency gravity wave energy. Putting Loon values into the *Schoeberl et al*. [2016] model increases cirrus fraction by ~70% compared to model results with no gravity waves. This puts the cloud fraction higher than the range of CALIOP observations shown in *Schoeberl et al*. [2016] (Figures 6 and 7). Consistent with these results, *Jensen et al*. [2016] used PreConcordiasi balloon measurements of temperature perturbations and found that homogeneous freezing driven by high-frequency waves produced higher ice concentrations than were observed in recent high-altitude aircraft campaigns. The discrepancy with observations can be resolved, however, if the amplitude of the gravity wave temperature spectrum (T'_o) decreases at lower altitudes following the observations reported by *Kim and Alexander* [2013]. These studies will be reported in a publication currently in preparation.

Acknowledgments
This work was supported under NASA grant NNX13AK25G and from the NASA Modeling, Analysis and Prediction program. Loon data are available from the Project Loon team. Please contact Rob Carver, carver@x.team. MERRA-2 data can be downloaded from the NASA GES DISC (https://disc.gsfc.nasa.gov/datareleases/merra_2_data_release). We thank Joan Alexander for her helpful comments on this manuscript. We would also like to thank two of the reviewers, Adrian McDonald and Julio Bacmeister, for their additional comments and suggestions.

References

Alexander, M. J. (1998), Interpretations of observed climatological patterns in stratospheric gravity wave variance, *J. Geophys. Res.*, *103*, 8627–8640.

Alexander, S. P., A. R. Klekociuk, A. J. McDonald, and M. C. Pitts (2013), Quantifying the role of orographic gravity waves on polar stratospheric cloud occurrence in the Antarctic and the Arctic, *J. Geophys. Res. Atmos.*, *118*, 11,493–11,507, doi:10.1002/2013JD020122.

Bacmeister, J. T., S. D. Eckermann, P. A. Newman, L. Lait, K. R. Chan, M. Loewenstein, M. H. Proffitt, and B. L. Gary (1996), Stratospheric horizontal wavenumber spectra of winds, temperature, and atmospheric tracers observed by high-altitude aircraft, *J. Geophys. Res.*, *101*, 9411–9470.

Baumgaertner, A. J. G., and A. J. McDonald (2007), A gravity wave climatology for Antarctica compiled from challenging Minisatellite Payload/Global Positioning System (CHAMP/GPS) radio occultations, *J. Geophys. Res.*, *112*, D05103, doi:10.1029/2006JD007504.

Boccara, G., A. Hertzog, R. A. Vincent, and F. Vial (2008), Estimation of gravity-wave momentum fluxes and phase speeds from quasi-Lagrangian stratospheric balloon flights. Part I: Theory and simulations, *J. Atmos. Sci.*, *65*, 3042–3055, doi:10.1175/2008JAS2709.1.

Bosilovich, M. G., et al. (2015), MERRA-2: Initial evaluation of the climate. NASA Tech. Rep. Series on Global Modeling and Data Assimilation, NASA/TM-2015-104606, vol. 39, NASA, 136 pp.

Dewan, E. M. (1994), The saturated-cascade model for atmospheric gravity wave spectra, and the wavelength-period (W-P) relations, *Geophys. Res. Lett.*, *21*, 817–820.

Dewan, E. M., W. Pendleton, M. Grossbard, P. Espy, and P. (1992), Mesospheric OH airglow temperature fluctuations: A spectral analysis, *Geophys. Res. Lett.*, *19*, 597–600.

Dinh, T., A. Podglajen, A. Hertzog, B. Legras, and R. Plougonven (2016), Effect of gravity wave temperature fluctuations on homogeneous ice nucleation in the tropical tropopause layer, *Atmos. Chem. Phys.*, *16*, 35–46, doi:10.5194/acp-16-35-2016.

Eckermann, S. D. (1999), Isentropic advection by gravity waves: Quasi-universal M3 vertical wavenumber spectra near the onset of instability, *Geophys. Res. Lett.*, *26*, 201–204.

Friedrich, L. S., A. J. McDonald, G. E. Bodeker, K. E. Cooper, J. Lewis, and A. J. Paterson (2017), A comparison of loon balloon observations and stratospheric reanalysis products, *Atmos. Chem. Phys.*, *17*, 855–866, doi:10.5194/acp-17-855-2017.

Fritts, D. C., and M. J. Alexander (2003), Gravity wave dynamics and effects in the middle atmosphere, *Rev. Geophys.*, *41*(1), 1003, doi:10.1029/2001RG000106.

Fritts, D. C., and G. D. Nastrom (1992), Sources of mesoscale variability of gravity waves. Part II: Frontal, convective, and jet stream excitation, *J. Atmos. Sci.*, *49*, 111–127.

Fritts, D. C., and T. E. VanZandt (1993), Spectral estimates of gravity wave energy and momentum fluxes, I: Energy dissipation, acceleration, and constraints, *J. Atmos. Sci.*, *50*, 3685–3694.

Fueglistaler, S., A. E. Dessler, T. J. Dunkerton, I. Folkins, Q. Fu, and P. W. Mote (2009), The tropical tropopause layer, *Rev. Geophys.*, *47*, RG1004, doi:10.1029/2008RG000267.

Gage, K. S. (1979), Evidence for a $k^{5/3}$ law inertial range in mesoscale two dimensional turbulence, *J. Atmos. Sci.*, *36*, 1950–1954.

Hertzog, A., and F. Vial (2001), A study of the dynamics of the equatorial lower stratosphere by use of ultra-long-duration balloons: 2. Gravity waves, *J. Geophys. Res.*, *106*(D19), 22,745–22,761, doi:10.1029/2000JD000242.

Hertzog, A., G. Boccara, R. A. Vincent, and F. Vial (2008), Estimation of gravity-wave momentum fluxes and phase speeds from quasi-Lagrangian stratospheric balloon flights. Part II: Results from the Vorcore Campaign in Antarctica, *J. Atmos. Sci.*, *65*, 3056–3070, doi:10.1175/2008JAS2710.1.

Jensen, E., and L. Pfister (2004), Transport and freeze-drying in the tropical tropopause layer, *J. Geophys. Res.*, *109*, D02207, doi:10.1029/2003JD004022.

Jensen, E. J., L. Pfister, and T. P. Bui (2012), Physical processes controlling ice concentrations in cold cirrus near the tropical tropopause, *J. Geophys. Res.*, *117*, D11205, doi:10.1029/2011JD017319.

Jensen, E. J., et al. (2016), High-frequency gravity waves and homogeneous ice nucleation in tropical tropopause layer cirrus, *Geophys. Res. Lett.*, *43*, 6629–6635, doi:10.1002/2016GL069426.

Kärcher, B., A. Dörnbrack, and I. Sölch (2014), Supersaturation variability and cirrus ice crystal size distributions, *J. Atmos. Sci.*, *71*, 2905–2926, doi:10.1175/JAS-D-13-0404.1.

Kim, J.-E., and M. J. Alexander (2013), A new wave scheme for trajectory simulations of stratospheric water vapor, *Geophys. Res. Lett.*, *40*, 5286–5290, doi:10.1002/grl.50963.

Kim, J.-E., and M. J. Alexander (2015), Direct impacts of waves on tropical cold point tropopause temperature, *Geophys. Res. Lett.*, *42*, 1584–1592, doi:10.1002/2014GL062737.

Massman, W. J. (1978), On the nature of vertical oscillations of constant volume balloons, *J. Appl. Meteorol.*, *17*, 1351–1356, doi:10.1175/1520-0450-1978.

Molod, A., L. Takacs, M. Suarez, J. Bacmeister, and J. (2015), Development of the GEOS-5 atmospheric general circulation model: Evolution from MERRA to MERRA2, *Geosci. Model Dev.*, *8*, 1339–1356, doi:10.5194/gmd-8-1339-2015.

Orr, A., J. S. Hosking, L. Hoffmann, J. Keeble, S. M. Dean, H. K. Roscoe, N. L. Abraham, S. Vosper, and P. Braesicke (2015), Inclusion of mountain-wave-induced cooling for the formation of PSCs over the Antarctic Peninsula in a chemistry-climate model, *Atmos. Chem. Phys.*, *15*, 1071–1086, doi:10.5194/acp-15-1071-2015.

Podglajen, A., A. Hertzog, R. Plougonven, and N. Žagar (2014), Assessment of the accuracy of (re)analyses in the equatorial lower stratosphere, *J. Geophys. Res. Atmos.*, *119*, 11,166–11,188, doi:10.1002/2014JD021849.

Podglajen, A., A. Hertzog, R. Plougonven, and B. Legras (2016), Lagrangian temperature and vertical velocity fluctuations due to gravity waves in the lower stratosphere, *Geophys. Res. Lett.*, *43*, 3543–3553, doi:10.1002/2016GL068148.

Rabier, F., et al. (2010), The Concordiasi project in Antarctica, *Bull. Am. Meteorol. Soc.*, *91*(1), 69–86, doi:10.1175/2009BAMS2764.1.

Schoeberl, M. R., A. E. Dessler, T. Wang, M. A. Avery, and E. J. Jensen (2014), Cloud formation, convection, and stratospheric dehydration, *Earth Space Sci.*, *1*, 1–17, doi:10.1002/2014EA000014.

Schoeberl, M. R., E. J. Jensen, and S. Woods (2015), Gravity waves amplify upper tropospheric dehydration by clouds, *Earth Space Sci.*, *2*, 485–500, doi:10.1002/2015EA000127.

Schoeberl, M., A. Dessler, H. Ye, T. Wang, M. Avery, and E. Jensen (2016), The impact of gravity waves and cloud nucleation threshold on stratospheric water and tropical tropospheric cloud fraction, *Earth Space Sci.*, *3*, 295–305, doi:10.1002/2016EA000180.

Smith, S. A., D. C. Fritts, and T. E. Van Zandt (1987), Evidence for a saturated spectrum of atmospheric gravity waves, *J. Atmos. Sci.*, *44*, 1404–1410.

Spichtinger, P., and M. Krämer (2013), Tropical tropopause ice clouds: A dynamic approach to the mystery of low crystal numbers, *Atmos. Chem. Phys.*, *13*(19), 9801–9818, doi:10.5194/acp-13-9801-2013.

Ueyama, R., E. J. Jensen, L. Pfister, and J.-E. Kim (2015), Dynamical, convective, and microphysical control on wintertime distributions of water vapor and clouds in the tropical tropopause layer, *J. Geophys. Res. Atmos.*, *120*, 10,483–10,500, doi:10.1002/2015JD023318.

Vincent, R. A., and A. Hertzog (2014), The response of superpressure balloons to gravity wave motions, *Atmos. Meas. Tech.*, *7*, 1043–1055, doi:10.5194/amt-7-1043-2014.

Vincent, R. A., A. Hertzog, G. Boccara, and F. Vial (2007), Quasi-Lagrangian superpressure balloon measurements of gravitywave momentum fluxes in the polar stratosphere of both hemispheres, *Geophys. Res. Lett.*, *34*, L19804, doi:10.1029/2007GL031072.